Uncertainty Quantification of Artemis I Space Launch System Integrated Aerodynamics Databases

Michael W. Lee*, Patrick R. Shea*, Jeremy T. Pinier†, and David T. Chan*
NASA Langley Research Center, Hampton, VA

Accurate prediction of integrated aerodynamic forces and moments is a necessary part of aerospace vehicle development. This accuracy can be quantified in the form of an uncertainty model, which makes the prediction more useful within an integrated vehicle design effort. Aerodynamic force and moment databases were constructed for the Artemis I mission of the Space Launch System vehicle. These databases reconcile data from multiple sources to yield unified predictions of how NASA's most advanced launch vehicle interacts with Earth's atmosphere as it ascends into orbit. This paper outlines how the uncertainty quantification was performed for these databases to ensure comprehensive and tractable uncertainty source coverage.

Nomenclature

$\mathcal{D}$	=	database model functional representation
d_2	=	bias correction factor for the range method
F	=	uncertainty factor
$\mathcal{M}$	=	mission stage functional representation
N	=	number of measurements in a repeated sample set
$\vec{p}$	=	parameter space vector, e.g., (α, β)
$\vec{q}$	=	vector of quantities of interest, e.g., axial, side, and normal integrated forces
R	=	range of residuals between multiple data sources
$\bar{R}$	=	range of residuals averaged over the parameter space
$\vec{u}$	=	vector of one uncertainty source for all quantities of interest
α	=	body-centric aerodynamic incidence angle
α_T	=	missile-axis (total) aerodynamic incidence angle
β	=	body-centric aerodynamic sideslip angle
σ	=	standard deviation

*Research Aerospace Engineer, Configuration Aerodynamics Branch, NASA Langley Research Center, AIAA Member.
†Research Aerospace Engineer, Configuration Aerodynamics Branch, NASA Langley Research Center, AIAA Associate Fellow.

Abbreviations

ARC	=	NASA Ames Research Center
AUPWT	=	ARC Unitary Plan Wind Tunnel
BPSWT	=	Boeing Polysonic Wind Tunnel
CFD	=	Computational Fluid Dynamics
F&M	=	Forces and Moments
LaRC	=	NASA Langley Research Center
LUPWT	=	LaRC Unitary Plan Wind Tunnel
MC	=	Monte Carlo
MPCV	=	Multi-purpose Crew Vehicle
MSFC	=	NASA Marshall Space Flight Center
NASA	=	National Aeronautics and Space Administration
RM	=	Range Method of approximating a standard deviation
SLS	=	Space Launch System
SM	=	Service Module
UQ	=	Uncertainty Quantification

I. Introduction

Aerodynamic databases perform a crucial function in the design of launch vehicles like the Space Launch System (SLS) [1]. Especially with vehicles whose first flight is also its first mission, the physics at play throughout the flight profile must be assessed from all viable perspectives, lest the cargo and crew be at more risk than has been anticipated. But every prediction has its own band of likely variation: its uncertainty. With any large-scale design effort, the complexity of the system can make the uncertainty space intractable without proper attention. This stems from the fact that different vehicle characteristics must be predicted independently. While these predictions are properly dependent on one another, that interdependence cannot be reconciled during the individual prediction efforts.

This reconciliation is instead performed by integrated multidegree-of-freedom Monte Carlo (MC) trajectory simulations [2–4]. The MC approach is well established [5–7]; it enables multiple, often disparate inputs that collectively characterize a system of interest to yield a coherent distribution of likely outputs. In other words, multiple prior distributions (e.g., aerodynamic forces on vehicle components, rocket engine thrust models, and structural deformation estimates) are fused through the system of governing equations to yield a single vector of posterior distributions (e.g., multiple possible rocket trajectories to orbit as a function of time).

The SLS design cycle quantifies all known uncertainties introduced within each of these independent prediction sets:

the requisite priors for the MC simulations. The reasoning is straightforward: rigorous accounting for uncertainties within each data source will yield a rigorous distribution of vehicle behavior via the MC simulations. Without quality priors, quality posteriors are unobtainable.

Aerodynamic force and moment (F&M) databases – the focus of this paper – are one category of vehicle trajectory MC inputs [8, 9].* The databases must anticipate how the vehicle interacts with the atmosphere on an integrated level: the net, six degree-of-freedom loading induced by the external aerodynamics and the rocket engines. Due to the nonlinearity of the mission fluid flows, which range in category from high-incidence subsonic regimes to multibody engine plume-dominated supersonic regimes to chemically active hypersonic regimes, the F&M predictions require a great deal of high-fidelity data to be collected [10]. The uncertainty of these data must be quantified to be 1) as comprehensive as possible and 2) compatible with the MC integration process.

More than a decade of effort yielded aerodynamic F&M databases – among many others – rigorous enough that the successful Artemis I mission in November 2022 flew nominally through the MC-simulated trajectory window. In this paper, the uncertainty quantification procedure for all SLS Artemis I aerodynamic F&M databases will be outlined. In Section II, all utilized data sources will be outlined and the nature of their uncertainty quantification will be discussed. In Section III, the individual Artemis I aerodynamic F&M database uncertainty models will be detailed. It will be shown that, although a unified UQ philosophy was applied across all presented databases, each database yielded a different – though structurally identical – uncertainty model.

II. Data and Uncertainty Sources

Uncertainty for all Artemis I SLS aerodynamic databases are regarded to stem from three sources, which collectively separate reality from the database representation. As outlined in Figure 1, these sources are representation error, sampling error, and database assembly error. Both epistemic and aleatoric uncertainties can be quantified within each of these steps, depending on which processes are employed. Whereas measurable uncertainties yield nominal value variances, which can be combined via a root-sum of squares when they are assumed to be independent, the relative fidelity of those variances is accounted for with uncertainty factors $F \geq 1$ that scale the variances within the total model. Uncertainty sources may differ in form and significance depending on what data are used to generate a database. For wind tunnel test data, representation error is usually small as long as the tunnel can match the flight conditions while sampling error may be larger due to calibration and repeatability errors; in contrast, for computational data, representation error is usually larger due to the approximation of the flow physics while sampling error is usually very small because the simulation can be recorded with numerical precision. Database assembly error tends to increase with database scope: the more (potentially disparate) flow physics a single database must capture, the more its assembly

*Although the SLS design effort employs aerodynamic databases that do not comprise integrated forces and moments, these non-F&M databases are out of the scope of this paper.

process will influence the total uncertainty.

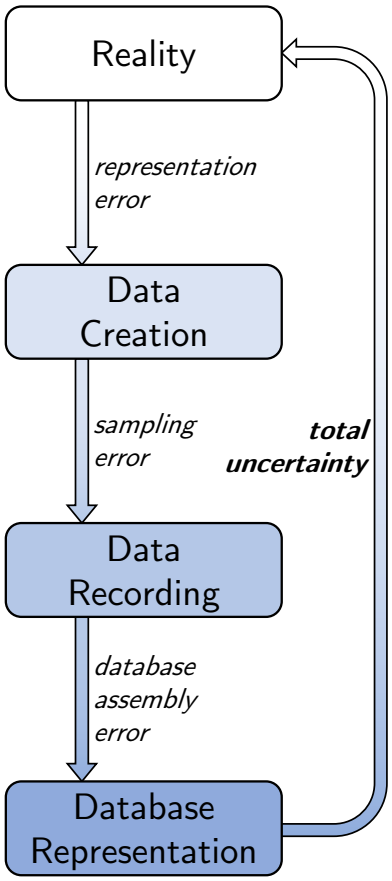

Fig. 1 Representation of uncertainty sources that separate an aerodynamic database from the reality that it strives to represent.

For SLS aerodynamic databases, only output uncertainties are measured to capture these three major error sources. An alternative process would be to directly quantify uncertainty due to data source-specific inputs, e.g., wind tunnel flow uniformity or a simulation grid resolution. Output uncertainties were selected over input uncertainties because of the many data sources employed across the myriad databases and the resulting uncertainty quantification procedure consistency. Such a decision naturally mandates that the outputs capture an acceptable spectrum of inputs; this was ensured on a data source-by-data source basis. For example, a wind tunnel repeatability uncertainty, which captures the experimental representation error, stems from observations at repeated conditions that are dispersed throughout the test matrix, or even across several tests, such that a spectrum of test condition deviations collectively inform the resulting output differences. This procedure is consistent with the general methodology developed during the Ares I program [11, 12].

A. Data Creation and Recording

While data creation focuses on obtaining nominal aerodynamic F&M values, the creation process itself introduces quantifiable uncertainty sources. Data sources can be loosely gathered into three categories: experimental data, namely from wind tunnel tests; computational data from physics-based simulations; and flight data from a relevant vehicle. In the case of the SLS, no relevant flight data existed prior to its first (successful) flight in November 2022. As such, the aerodynamic F&M databases were based solely on experimental and computational data.

1. Experimental Data

Nominal data were collected in several wind tunnels: the Langley Research Center (LaRC) 14- by 22-Foot Subsonic Tunnel (14×22), the Ames Research Center (ARC) Unitary Plan Wind Tunnel (AUPWT), and the Boeing Polysonic Wind Tunnel (BPSWT). Additional wind tunnel tests were conducted in the Marshall Space Flight Center (MSFC) 14-inch Trisonic Wind Tunnel and the LaRC Unitary Plan Wind Tunnel (LUPWT) to support uncertainty quantification. Select test model images are shared in Figure 2.

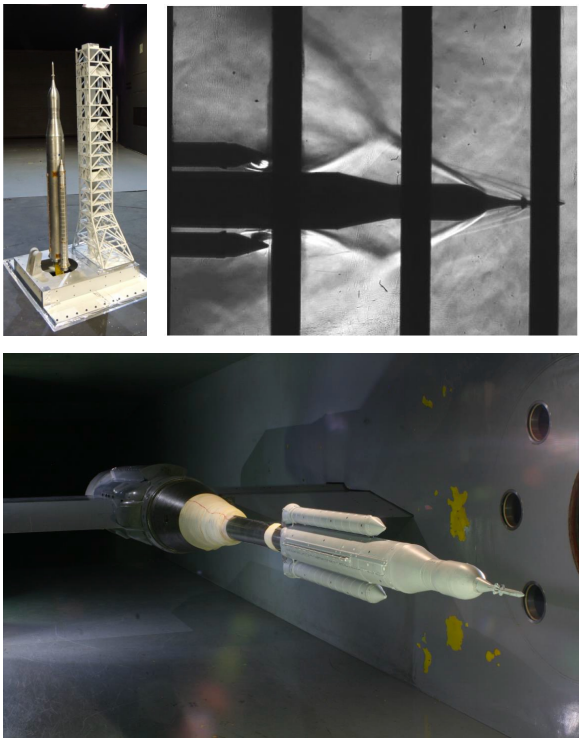

Fig. 2 SLS wind tunnel test models in the LaRC 14×22-foot tunnel (top left) and the AUPWT (bottom) and a mid-test schlieren image of the test model in the LUPWT (top right) [Source: NASA].

Each wind tunnel follows its own data management protocols due to differences in facility functionality, data acquisition hardware, and test objectives. While the SLS tests obtained the aerodynamic F&M data relevant to this paper, in many cases a single wind tunnel test gathers data for multiple objectives at the same time; e.g., surface pressure

estimates via pressure-sensitive paint to reinforce distributed loads databases used in structural analyses.

Despite the idiosyncrasies of testing one launch vehicle in disparate wind tunnel facilities, the manner by which the experimental data uncertainty is quantified generally follows the same protocols [13, 14]. Force balance calibration uncertainty, the principal sampling uncertainty as defined in Figure 1, is computed by a controlled measurement of known loads to capture 2σ deviations between applied and measured values; these are extended to be 3σ bounds in agreement with SLS standards:

$$\vec{u}_{cal} = 3\sigma_{cal} \ . \tag{1}$$

The principal wind tunnel representation uncertainty is captured with replicated components of the test matrix: capturing data at the same prescribed conditions multiple times and characterizing the differences in measured loads. While some repeat runs are adjacent within the test matrix, other repeats are intentionally dispersed to provide a spectrum of input alterations. This characterization is performed with a process known as the range method (RM).

Standard Deviations via the Range Method (RM) The range method is a technique founded in statistical process control [15]. It is a method by which standard deviations of many samples can be estimated from the ranges of few samples. The process is as follows:

1) interpolate data gathered at comparable conditions to numerically identical conditions, e.g., for two quantity of interest vectors in the $(\alpha\,, \beta)$ space

$$\left.\begin{matrix} \vec{q}_1(4.27,\ -3.08) \\ \vec{q}_2(4.31,\ -3.13) \end{matrix}\right\} \rightarrow\ \vec{q}_{1,2}(4.3, -3.1)\ ;$$

2) compute the average range of residuals within data groups of interest, e.g., from a residual range space $R(\alpha, \beta) = |\vec{q}_1 - \vec{q}_2|$ all β measurements may be averaged together to yield an average residual range space $\bar{R}(\alpha)$;
3) approximate the standard deviation of the measurement variations by normalizing the average measurement residual ranges with a coefficient d_2

$$\sigma_{RM} = \frac{\bar{R}}{d_2} \tag{2}$$

where d_2 is determined based on how many measurements N were used to compute the residual range [15]:

$$d_2(N = 2,\ 3,\ 4,\ 5) = (1.128,\ 1.693,\ 2.059,\ 2.326)\ .$$

In the example case where two repeated measurements $\vec{q}_{1,2}$ determine the residual range, $d_2 = 1.128$ would be employed. The final step is to then

4) multiply the computed standard deviation by three to determine the data repeatability uncertainty:

$$\vec{u}_{rep} = 3\sigma_{RM} \ . \tag{3}$$

Additional uncertainty factors are applied to account for unmodeled effects and additional uncertainty terms may be introduced on a test-by-test basis (e.g., uncertainty introduced by fusing data from multiple tunnel tests), but the calibration and repeatability uncertainties are mainstays of experimental data uncertainty quantification for all SLS aerodynamic F&M databases.

2. Computational Data

When available experimental data sources cannot meet the requirements for a particular database, computational sources instead provide nominal aerodynamic loads. For Artemis I F&M databases, the Cart3D inviscid flow solver [16] provided all nonexperimental nominal data. The FUN3D [17], OVERFLOW [18], and Loci/Chem [19, 20] tools provided additional data used in uncertainty quantification.

Cart3D is a structured-Cartesian-grid, inviscid flow solver with the capability to simulate flow physics in subsonic, transonic, supersonic, and hypersonic flow regimes. The relatively low computational cost, paired with grid adaptation capabilities, enables this solver to interrogate a very large parameter space with acceptable accuracy as well as acceptable cost. An example of Cart3D grid refinement, in this case within the ascent stage discussed more fully in Section III.B, is shown in Figure 3.

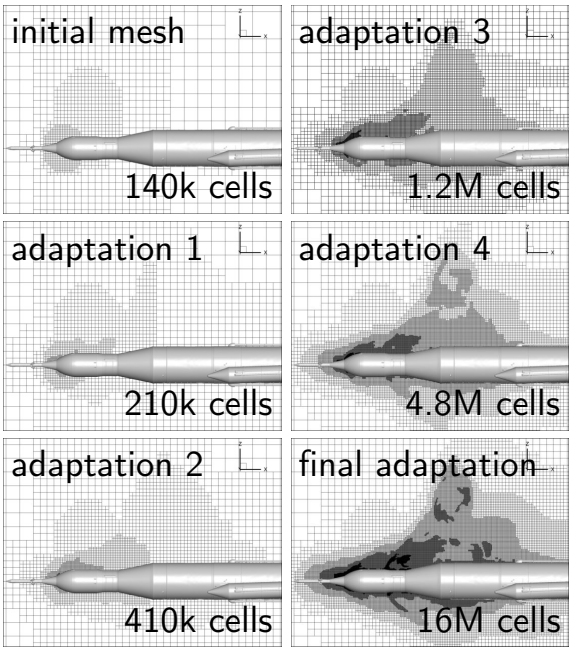

Fig. 3 An example of Cart3D grid refinement for flow around the SLS within the ascent mission stage.

Output uncertainties, rather than input uncertainties, were measured for computational data sources. Computational data input uncertainty quantification has been and remains an active area of research [21–24], but for SLS aerodynamic databases such procedures were not implemented. Standard efforts such as grid resolution studies and turbulence model comparisons were performed to substantiate the delivered data, but such efforts did not inform the uncertainty model. Rather, similar flow conditions were simulated with multiple architectures – both computational and experimental, where applicable – in order to assess the Cart3D predictive fidelity at an integrated level. Within these different architectures, variations in grid resolution, grid adaptation, turbulence modeling, the inclusion of viscous effects, etc. collectively informed differences in simulation outputs, which directly informed the uncertainty models. For example, it is understood that OVERFLOW is a higher-fidelity viscous flow solver than Cart3D, but its higher computational cost may not fit with the demands of a particular database. An example of the OVERFLOW grid adaptation and contours of viscous, plume-affected flow solutions is presented in Figure 4.

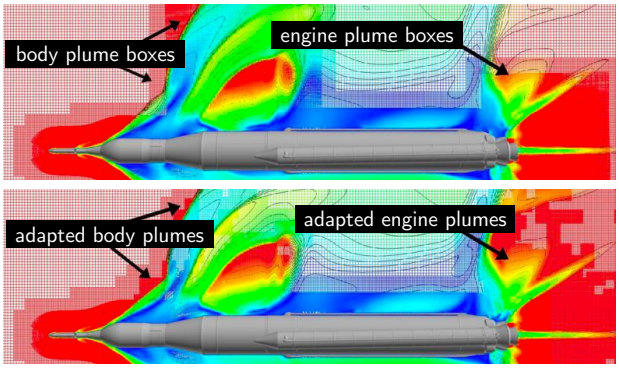

Fig. 4 An example of OVERFLOW initial (top) and subsequent (bottom) grid refinement and notable flow characteristics for flow around the SLS within the ascent mission stage.

To assess the significance of the differences in Cart3D and other representations of reality, the resulting force and moment coefficients can be compared at a small number of parameter points more obtainable with higher-fidelity tools and the resulting variations generalized to the entire data space. In the case of comparing to a wind tunnel test, this means that Cart3D is set to replicate tunnel conditions instead of flight conditions for a more proper comparison. Quantifying uncertainties from these code-to-code or code-to-tunnel comparisons accounts for the significant representation errors inherent in flow simulation, as introduced in Figure 1 and is again computed with the RM.

B. Database Representations

Aerodynamic databases can be regarded as models for the loads of interest, which are defined continuously within the parameter space that spans a particular mission stage. Given a state vector $\vec{p}$ (e.g., Mach number and body-centric incidence angles α and β) within the mission stage $\mathcal{M}$, the database $\mathcal{D}$ returns a vector of nominal quantities of interest

$\vec{q}_n$ (e.g., total side and normal forces) and centered uncertainty margins $\vec{q}_u$ for those quantities.

$$\mathcal{D}(\vec{p}) = \vec{q}_n \pm \vec{q}_u \quad \forall\, \vec{p} \in \mathcal{M} \tag{4}$$

These models are built using a finite amount of data, often from several data sources. The model fuses these myriad discrete data sources into a single, unique-valued, continuous field of quantities of interest.

1. Response Surface Modeling

A response surface is a continuous quantity of interest field that is based on a sparse, discrete data set [25]. An example is shown in Figure 5. Based on one of several possible continuous mathematical functions, the response surface warps to fit all provided data within user-specified tolerances. For the liftoff and transition and ascent databases, a natural interpolant was employed; for the booster separation database, because the Voronai diagram is ill-conditioned in high dimensions, kriging was employed instead. The response surface can be fit to data from multiple sources, which enables data fusion to be performed by the surface definition itself. The surface can then be sampled at much higher resolution in the parameter space than is possible with the original data sources to yield deliverable, high-resolution data tables.[†]

As with other data-driven modeling techniques, it is standard practice to omit a fraction of the source data from the response surface creation process [25]. Checking the response surface against these omitted data yields a quantification of the surface predictive fidelity: how well it anticipates the quantities of interest where it was not given reference data. If the response surface was not forced to pass through the training data as well, i.e., a higher fit tolerance was allocated, then the training data also provides a quantification of predictive fidelity. The number of training and test points varied from database to database, as detailed in subsequent sections of this paper, but consistent alignment of training and testing point comparisons verified that an adequate number of points were generated. The response surface modeling uncertainty is quantified from the surface-data comparisons, as with previous steps, via the RM where only a small number of point comparisons are available.

2. Data Tabulation and Interpolation

In particularly large parameter spaces like the booster separation event database discussed in Section III.C, even tabulating a response surface with as high a resolution as is tractable yields a relatively sparse database. The interpolation of this sparse data space by the trajectory simulation codes may differ from the response surface predictions, and this additional uncertainty source, where significant, must be accounted for. Test points and the RM are used to perform this quantification just as they were used to quantify the response surface modeling uncertainty.

[†]Program requirements mandated the delivery of high-resolution data tables as opposed to response surfaces packaged, for example, within an application programming interface.

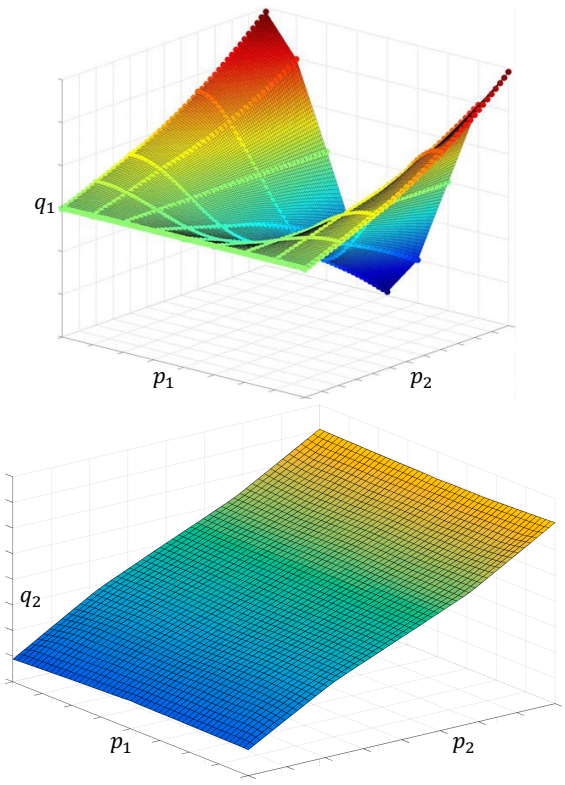

Fig. 5 Example response surfaces of two F&M coefficients (q_1 and q_2) defined within a two-dimensional parameter space (p_1 and p_2). Points (only shown on top plot) denote discrete data that defined the response surface.

III. Uncertainty Models throughout the Mission Profile

Several aerodynamic force and moment databases collectively cover the trajectory window through which the SLS exits the atmosphere. As outlined in Figure 6, the vehicle rises vertically off a mobile launch tower and performs an initial transitional roll maneuver, ascends at a relatively low incidence angle as its speed increases, separates its solid rocket boosters, continues to ascend and accelerate until the service module panels and launch abort system jettison, and then exits the atmosphere. The core stage separates after atmospheric effects are no longer significant; the launch abort system jettison is managed by the Orion capsule research team and is thus out of the scope of this paper [26]. As such, the service module panel jettison is the final mission milestone for which the SLS aerodynamics task team is responsible. The following sections outline the aerodynamic uncertainty models that cover these mission stages for the Artemis I flight.

A. Liftoff and Transition

The liftoff and transition mission stage sees the rocket separate from the tower and sweep from a high, wind-dominated angle of attack to a low, velocity-dominated angle of attack. It is worth noting that aerodynamic transition occurs as the rocket is lifting off and is not a function of ground-relative rocket pitch angle. Though entirely incompressible, the

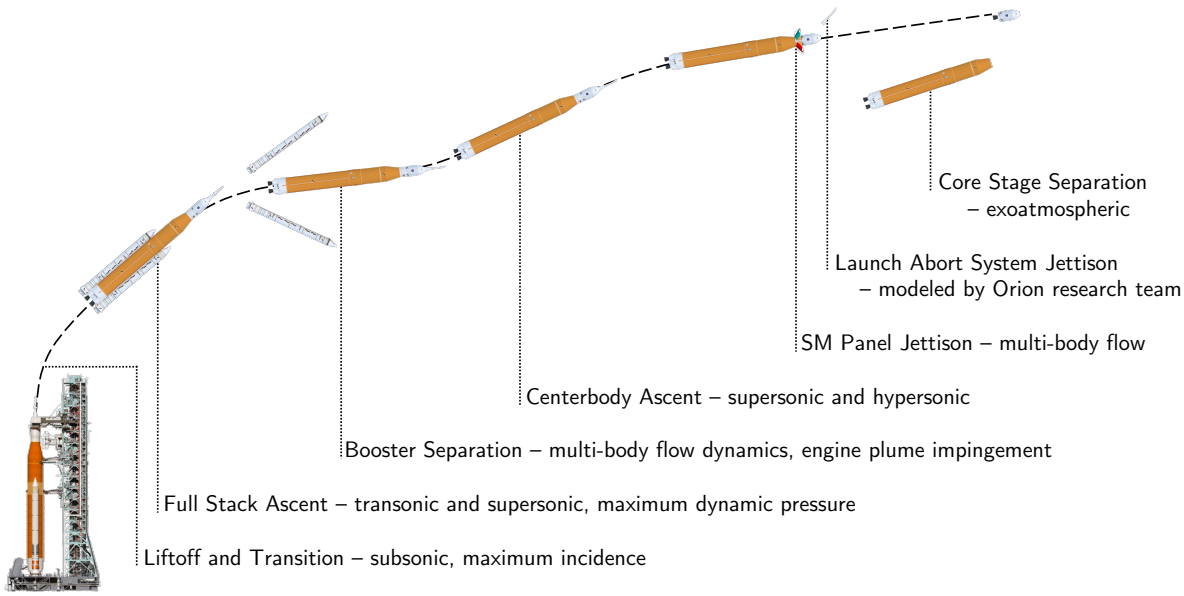

Fig. 6 Schematic of the Space Launch System Artemis I mission profile. Notable aerodynamic characteristics are noted alongside the mission stages.

aerodynamic data space is sizeable, with angles of attack and sideslip ranging from -90° to 90°. Data are provided for the integrated vehicle as well as for each booster individually. For the liftoff portion, the aerodynamic influence of the tower is accounted for.

This database is founded solely on data from the LaRC 14- by 22-foot Subsonic Tunnel (14×22) [27]. A simplified tower geometry was employed to reduce manufacturing costs without sacrificing test relevance. The booster loads were measured independently from the full-stack loads. Data symmetrization was utilized where tunnel data could not physically be collected in the liftoff portion. Natural interpolant response surfaces were generated from the collected data and then sampled for higher-resolution database tabulation.

Due to the single data source, the uncertainty model is relatively straightforward. In the transition portion, representation error and sampling error are collectively captured through balance calibration ($\vec{u}_{cal}$) and experiment repeatability ($\vec{u}_{rep}$) errors; modeling error ($\vec{u}_{mod}$) is captured by comparing the database response surface to the underlying wind tunnel measurements. Uncertainty factors for the experiment, F_{exp}, and the database tabulation, F_{db}, were included to account for aleatoric uncertainties.

$$\vec{q}_u^{\,transition} = \sqrt{F_{exp}\left(\vec{u}_{cal}^2 + \vec{u}_{rep}^2\right) + F_{db}\vec{u}_{mod}^2} \tag{5}$$

The calibration term was provided by a balance specification sheet. The repeatability term was computed via the RM. The response surface uncertainty was computed by comparing response surface values to exact tunnel measurements and taking a 3σ bound of the differences. All three components were computed within three separate total aerodynamic

incidence windows: 0°–20°, 30°–60°, and 70°–90°. As such, the total uncertainty is a function of the same α-β data space as is the nominal data table.

The liftoff model is structurally identical but introduces additional uncertainty terms for 1) the symmetry assumption needed to fill missing data ranges ($\vec{u}_{sym}$) and 2) the lateral vehicle-tower proximity that can vary due to vehicle drift during flight ($\vec{u}_{prx}$): respectively, additional epistemic and aleatoric uncertainties in the representation category. However, because the uncertainty due to vehicle drift was concluded to be perfectly correlated with balance calibration uncertainty, the balance calibration uncertainty was removed from the model and the repeatability uncertainty was doubled.

$$\vec{q}_u^{liftoff} = \sqrt{2F_{exp}\vec{u}_{rep}^2 + F_{db}\left(\vec{u}_{mod}^2 + \vec{u}_{sym}^2 + \vec{u}_{prx}^2\right)} \tag{6}$$

The symmetry term was computed by symmetrizing about different angles and comparing the resulting drift in trend. It is set to zero outside of the symmetrized data range. The tower proximity term was computed by taking additional data at slightly off-nominal lateral vehicle positions and applying a 3σ bound to the observed changes in aerodynamic loads.

In addition to providing conservative buffers on the uncertainty terms, the uncertainty factors account for unmodeled effects including differences between flight and wind tunnel Reynolds numbers, geometric differences between test and flight like the tunnel structure simplification, and engine plume effects.

Representative uncertainty buildups are presented in Figure 7. Different uncertainty sources contributed more significantly in different flight regions. Response surface modeling uncertainty was consistently lower or equivalent to the other sources. Repeatability was dominant through the higher-incidence data range, which is to be expected due to the complicated flow separation downstream of the vehicle. In the transition portion, calibration uncertainty was more influential at lower aerodynamic incidences. In the liftoff portion, tower proximity and symmetry uncertainties were both similar to the repeatability uncertainty in different F&M values.

B. Ascent

The ascent stage covers the rocket progression from the transition stage all the way up to where the atmosphere becomes rarefied and aerodynamics no longer play a significant role in the vehicle trajectory [28]. The flow proceeds from transonic to supersonic to hypersonic; the vehicle experiences its maximum dynamic pressure; the boosters and eventually the Multi-purpose Crew Vehicle (MPCV) panels separate from the centerbody as it proceeds to orbit. The aerodynamic incidence range is much more restricted than it is for the liftoff and transition database, but the Mach range is far larger. An overlap in Mach ranges exists for the full-stack and centerbody database sections to account for variable booster separation events.

The full-stack database was based on wind tunnel tests in the AUPWT and the BPSWT [29, 30]. Natural interpolant response surfaces were constructed from the wind tunnel data and interrogated to build the final data tables. The

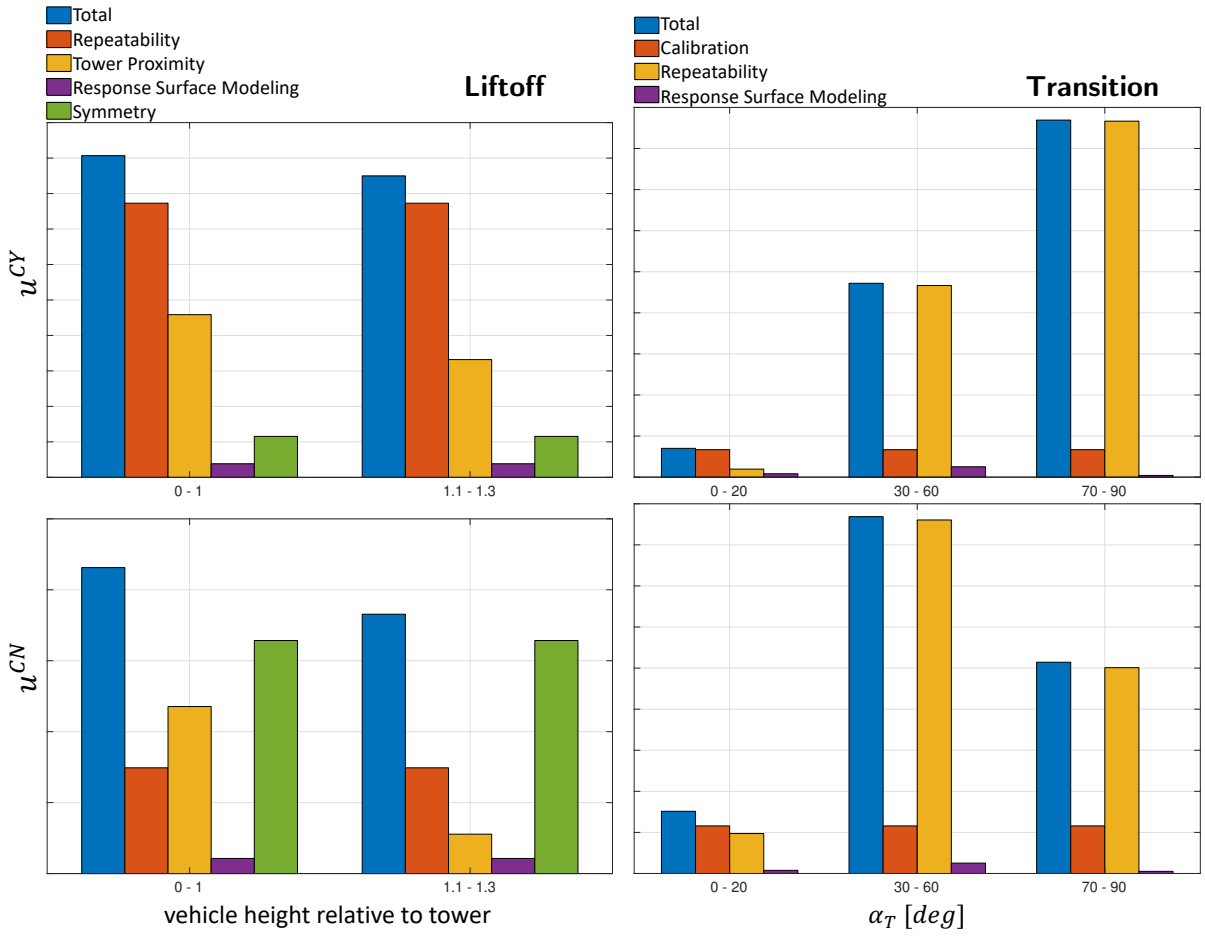

Fig. 7 Representative uncertainty component buildups for the liftoff (left) and transition (right) F&M database for side (u^{CY}, top) and normal forces (u^{CN}, bottom).

AUPWT data covered the lower end of the Mach range and the BPSWT covered the higher end. The overlapping Mach region served as a source for uncertainty quantification with the AUPWT data being treated as the nominal source. Simulations were conducted in FUN3D to augment the uncertainty model.

The centerbody database was constructed with over 1,000 inviscid simulations in the Cart3D solver distributed uniformly within the data space. Due to their lack of impingement on the vehicle, the exhaust plumes were not modeled. Due to the overall flow stability, pseudosteady rather than time-accurate Reynolds-averaged Navier-Stokes simulations were conducted.

The full-stack uncertainty model is more complicated than the transition model due to the multiple data sources. It comprises a buildup of balance calibration ($\vec{u}_{cal}$), test repeatability ($\vec{u}_{rep}$), response surface interpolation ($\vec{u}_{mod}$),

ground-to-flight ($\vec{u}_{G2F}$), and tunnel-to-tunnel ($\vec{u}_{T2T}$) uncertainties.

$$\vec{q}_u^{\,ascent,\ full\ stack} = F_{full\ stack}\sqrt{\begin{array}{c} 2\vec{u}_{cal}^2 + \vec{u}_{rep}^2 + \vec{u}_{mod}^2 \\ +\vec{u}_{G2F}^2 + \vec{u}_{T2T}^2 \end{array}} \tag{7}$$

An uncertainty factor was added outside of the root-sum of squares, rather than on a term-by-term basis, so that it would be structurally comparable to the uncertainty factor used in the centerbody uncertainty model described immediately below. Calibration and repeatability uncertainties were computed with the standard procedure [31, 32]; the calibration uncertainty was doubled to also account for in-test measurement adjustments, which are perfectly correlated with calibration uncertainty. These two terms were computed for the lower Mach range from the AUPWT data and for the higher range from the BPSWT data, due to those data sources providing the nominals in those ranges. The response surface modeling uncertainty is itself a root-sum of squares

$$\vec{u}_{mod}^2 = \vec{u}_{resub}^2 + \vec{u}_{interp}^2 \tag{8}$$

computed by comparing response surface values to 1) tunnel measurements provided for surface creation ($\vec{u}_{resub}$) and 2) tunnel measurements withheld during surface creation ($\vec{u}_{interp}$) and taking a 3σ bound of the differences in both cases. At some Mach ranges, *interp* data sets were unavailable. The observed differences between the response surfaces and the tunnel data were counterbalanced by the repeatability uncertainty to ensure that it is not double-counted within the model uncertainty; where $\vec{u}_{mod} < \vec{u}_{rep}$, the modeling uncertainty was set to zero. The ground-to-flight uncertainty, which accounts for differences between the tunnel conditions and those experienced by the full-scale vehicle, was computed by building two alternative response surfaces based on FUN3D data – one at tunnel conditions and another at flight conditions – and comparing them to one another and recording the 3σ-bounded difference. The tunnel-to-tunnel uncertainty captures the differences between tunnel measurements relative to the AUPWT data. As such, this term vanishes in the lower Mach range because the source data are from the AUPWT; the BPSWT-based higher-Mach range data have nonzero tunnel-to-tunnel uncertainties to account for this shift in source data. A small, global uncertainty factor was applied for conservatism.

A representative buildup of the full-stack ascent uncertainty terms is presented in Figure 8. The ground-to-flight uncertainty was dominant in most Mach ranges. The modeling and calibration uncertainties were more significant at lower Mach ranges, whereas the repeatability uncertainty varied in significance both across Mach ranges and between coefficients.

The centerbody uncertainty model only has one term: a code-to-tunnel uncertainty ($\vec{u}_{C2T}$) computed by comparing the Cart3D simulations to data from the MSFC 14-inch Trisonic wind tunnel. Directly measurable sampling errors in

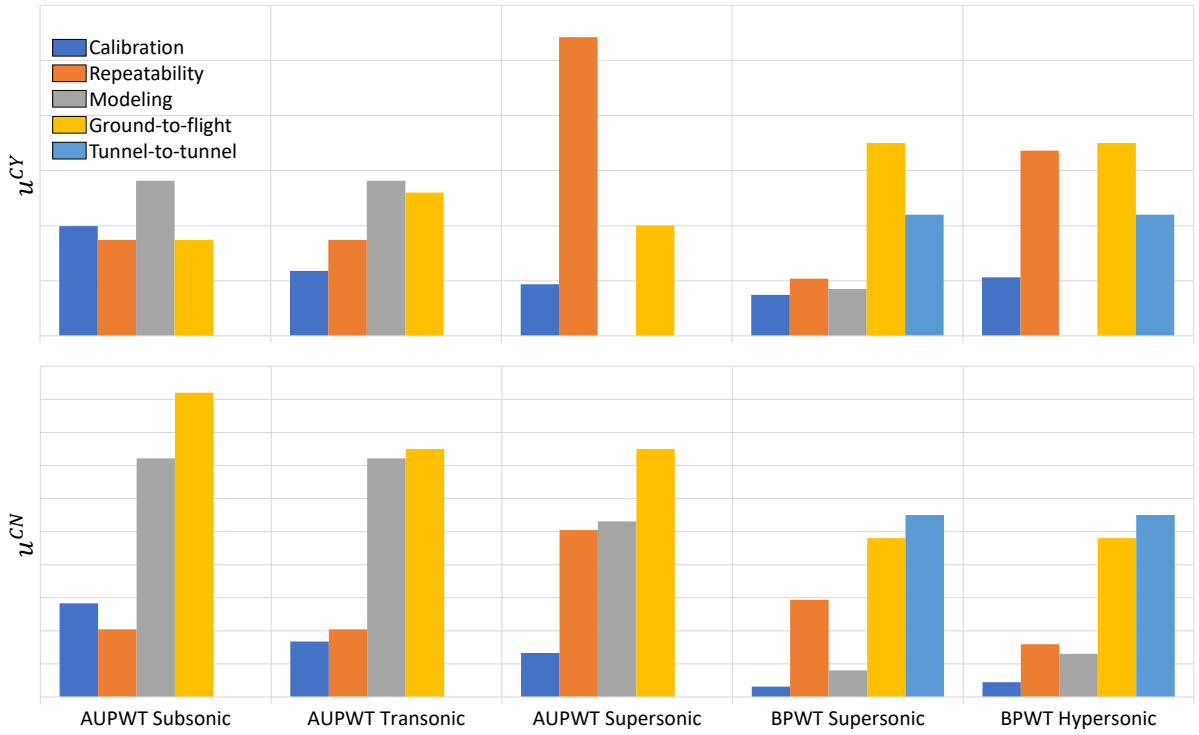

Fig. 8 Representative uncertainty component buildups for the full stack ascent F&M database for side (top) and normal forces (bottom).

the simulation were small enough that they were neglected. The Cart3D data were directly delivered as the database table, so no additional data modeling uncertainty was introduced. As such, the root sum square reduces to a single unsquared term.

$$\vec{q}_u^{\,ascent,\ centerbody} = F_{centerbody}\vec{u}_{C2T} \tag{9}$$

Unmodeled effects are accounted for with a more substantial uncertainty factor relative to the full-stack model.

C. Solid Rocket Booster Separation

The separation of the solid rocket boosters (SRBs) is a mission-critical event that occurs midway through the ascent stage. When the SRB thrust drops below a certain near-zero threshold, separation motors (on each SRB) fire from either side of the centerbody and the SRBs jettison outboard while the centerbody continues to accelerate forward. An outline of their general trajectory is shown in Figure 9. During this event, aerodynamic forces and moments influence whether the boosters will 1) successfully clear their mounting hardware, 2) avoid recontacting the centerbody as they move aft, and 3) avoid contacting each other as they impinge on the main engine plumes and fall back to Earth.

As outlined in Ref. [33], the booster separation database covers a very large parameter space in order to anticipate myriad booster separation trajectories. This broad space was populated with over 20,000 Cart3D simulations dispersed using a thirteen-dimension star-shaped approach with initially uniform point spacing in each dimension. Kriging defined

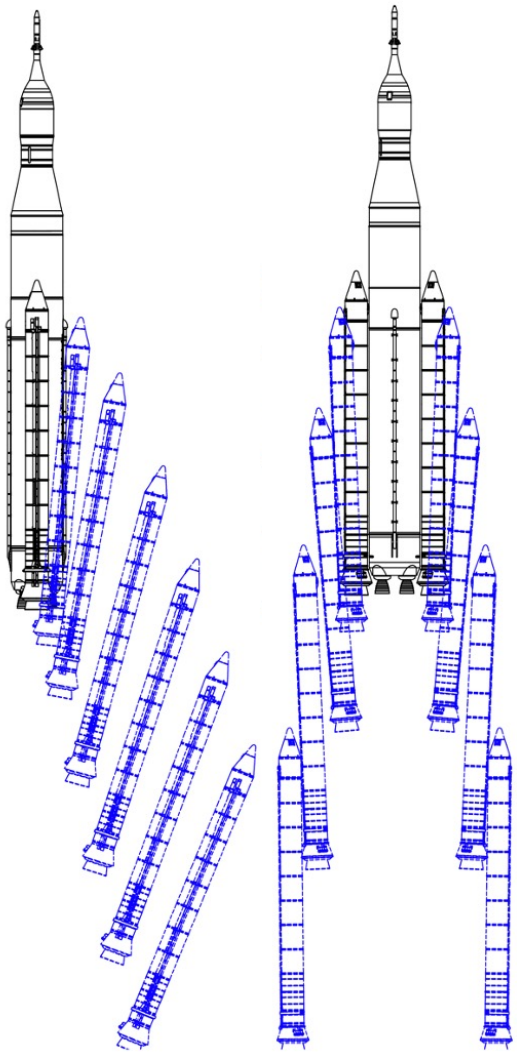

Fig. 9 An outline of the Artemis I booster separation event.

the response surface because the Voronai diagram that defines the natural neighbor interpolant was found to be poorly conditioned in such a high dimension. The Cart3D capability to model plume interactions was employed. The database also accounts for whether a core-stage engine or a booster separation motor are disabled due to a flight anomaly, to ensure that in these eventualities the off-nominal mission profiles are still viable.

The uncertainty was quantified by comparing Cart3D simulations to two other, lower-parameter resolution data sources: approximately 100 OVERFLOW simulations ($\vec{u}_{C2C}$) and approximately 6,000 Cart3D simulations replicating points in an LUPWT test ($\vec{u}_{C2T}$) [34]. Uncertainty was also quantified for the iteration averaging in Cart3D ($\vec{u}_{num}$), database tabulation procedure ($\vec{u}_{mod}$), and the assumption that the boosters could be simulated at symmetric separation positions but sampled independently of one another ($\vec{u}_{sym}$). An additional uncertainty term was included to account for the database structure and how it addressed booster separation motor failures ($\vec{u}_{bsm}$). This final uncertainty term was

excluded for database usage where the booster separation motors were nominal.

$$\vec{q}_u^{booster\ separation} = \sqrt{\begin{matrix} F_{cfd}\left(\vec{u}_{C2T}^2 + \vec{u}_{C2C}^2 + \vec{u}_{num}^2\right) \\ +F_{db}\left(\vec{u}_{mod}^2 + \vec{u}_{sym}^2 + \vec{u}_{bsm}^2\right) \end{matrix}} \tag{10}$$

The code-to-tunnel uncertainty was computed by taking a 3σ bound of point-to-point comparisons as a function of axial booster separation distance; the code-to-code uncertainty was computed via the RM because not enough points existed at each axial separation distance to make a statistically representative set. The Cart3D sampling error uncertainty came from a 3σ bound of variations in the simulation caused by simulating the same physical conditions with various computational settings including CFL number and initial mesh resolution. The response surface model error is especially important in this database due to the very high dimension of the parameter space; several dozen test points were simulated in Cart3D and compared to the response surface, bounding the results at 3σ to quantify this uncertainty source. Several thousand additional Cart3D simulations were conducted to quantify the effect of the symmetry assumption throughout the entire parameter space, with similar 3σ bounds on the results yielding the uncertainty term. Several dozen more were run to quantify the booster separation motor uncertainty. The total uncertainty was defined only as a function of the booster axial distance from its initial position.

A representative buildup of uncertainties on SRB forces is presented in Figure 10. Different uncertainty sources dominate different stages of the separation event. The uncertainty model dependency on the booster axial separation distance enables the F&M at smaller separation distances, where centerbody recontact is more likely, to be represented within a tighter yet still rigorous uncertainty margin that is not affected by the larger uncertainties that exist at larger separations. At all separation distances, the Cart3D numerical uncertainty is minimally influential in the nominal flight regime but far more dominant in the engine-out conditions. The inclusion of the booster separation motor uncertainty term tends to have more influence at the larger separation distances.

Moderate uncertainty factors were employed to account for unmodeled effects including untracked parameter sensitivities and unsteady effects. Additional validation was performed by 1) further assessing the rigor of the code-to-code uncertainty using a tertiary flow solver and 2) simulating booster movement directly within OVERFLOW, but these validation sets were not included in the uncertainty model due to double-counting.

D. MPCV SM Panel Jettison

The jettison of the Multi-purpose Crew Vehicle (MPCV) service module (SM) panels occurs at hypersonic Mach numbers near the altitude boundary where aerodynamic effects are no longer influential on the vehicle trajectory. A schematic of the jettison for one panel is provided in Figure 11. As with booster separation, the database is organized into multiple regions of aerodynamic similarity: the Hinged, Near, and Far domains. The panels must jettison prior to

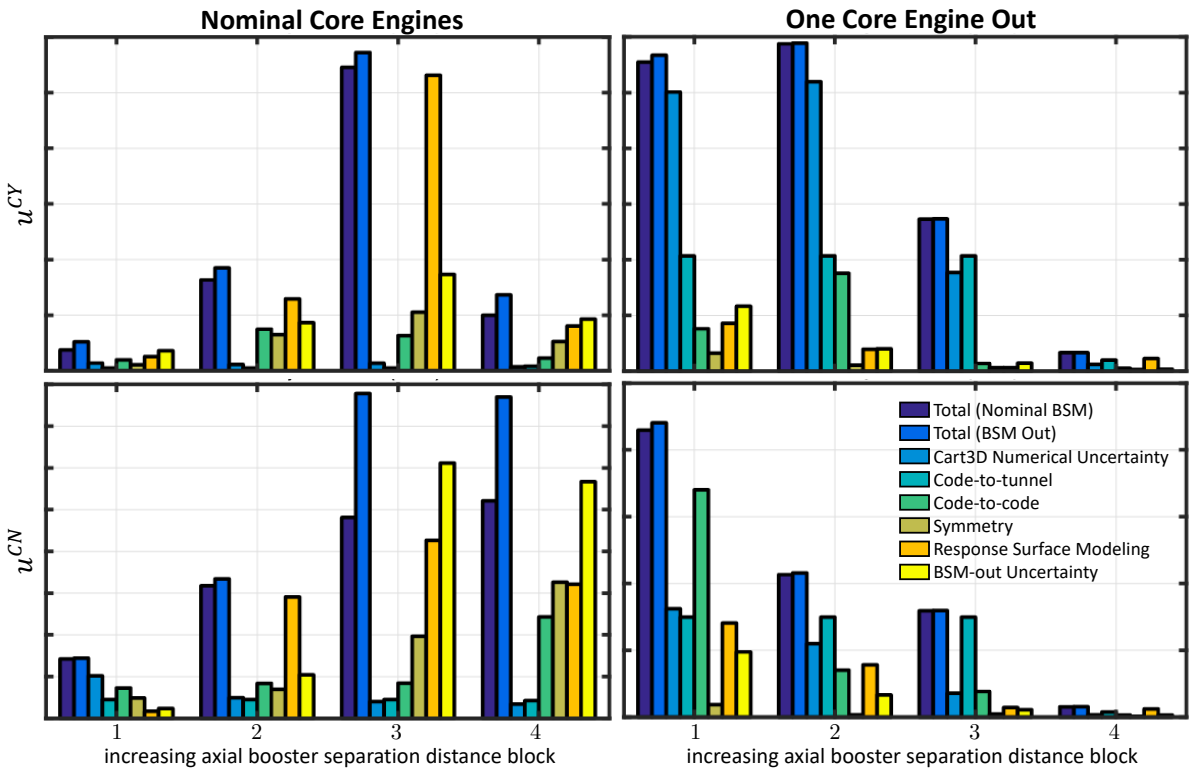

Fig. 10 Representative uncertainty component buildups for the nominal (left) and core engine-out (right) booster separation F&M database for SRB side (top) and normal forces (bottom). The SRBs are further downstream of the centerbody as the separation distance blocks increase from 1 to 4.

the MPCV separation from the centerbody; the aerodynamic database serves to ensure that they do not recontact with the centerbody during the jettison event.

In addition to simulating multiple panels at multiple positions, the database is a function of the centerbody angles of attack and sideslip. Due to the high parametric complexity and the multibody nature of the problem, as with booster separation, the primary data source for this database is the Cart3D flow solver.

This database uncertainty model only accounts for representation error and sampling error because the database assembly error was found to be negligible.

$$\vec{q}_u^{\,MPVC\ SM\ panel\ jettison} = \sqrt{F_{cfd}\left(\vec{u}_{C2C}^{\,2} + \vec{u}_{num}^{\,2}\right)} \tag{11}$$

The code-to-code (representation) uncertainty was quantified by comparing select (inviscid) Cart3D simulations to (viscous) Loci/Chem simulations and taking a 3σ bound of the identified differences. The numerical uncertainty was quantified directly from the fluctuations in the inviscid solution iteration history to a similar 3σ bound. In this and all other databases, grid resolution was studied to substantiate the delivered databases but the results did not inform the uncertainty model directly. The resulting uncertainties were collected into the three jettison regions but left uniform

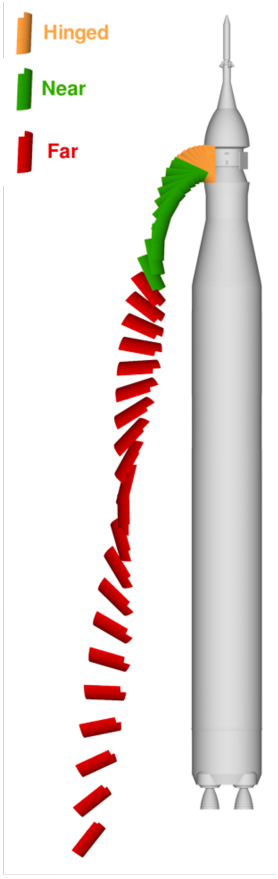

Fig. 11 An outline of the Artemis I MPCV SM panel jettison event. Note that one panel is illustrated but that multiple panels jettison at once on the actual vehicle.

within each region. They differed for each panel due to the interactions between panels and the centerbody orientation.

IV. Conclusion

In this paper, the uncertainty quantification procedures applied to the Space Launch System Artemis I configuration aerodynamic forces and moments databases have been summarized. Treatment of different data source types was discussed and each specific database was outlined.

Although each uncertainty model in Section III was unique, they were all created using the same core principles: accumulation of uncorrelated uncertainties; the range method to characterize uncertainties from sparse, comparable measurements; fair audits of both epistemic and aleatoric uncertainty sources that often affect the severity of uncertainty factors; and an awareness of how the resulting databases will interact with the rest of the vehicle program. These tenets yielded databases that were accurate enough for reasonable mission viability assessments to be performed and conservative enough for reasonable externalities to be anticipated.

Quantification of uncertainty in applied aerodynamic applications is an exercise in risk acceptance. These databases

exist within larger frameworks of vehicle design and risk mitigation; while the nominal aerodynamic loads tend to inform the configuration design, the uncertainties on those loads more significantly inform anticipated safety factors, launch windows, and ultimate configuration functionality. And yet the most useful and relevant aerodynamic database is not one that multiplies its bounds ad infinitum in the name of conservatism. Rather, it is crucial for aerodynamic database developers to provide accurate and precise representations of how the vehicle interacts with the air, all across the spectrum of relevant variations. Only then can the program at large conclude whether aerodynamically motivated concerns are valid ones; only then can the vehicle operate as expected.

Acknowledgments

The authors thank Dr. Robert Hall for his leadership of the Ares Aero Panel during the Ares rocket development period, as those efforts forged the foundation of the Space Launch System database development methodologies. The authors also thank Michael Hemsch, Amber Favaregh, and Heather Houlden for their efforts in developing uncertainty quantification standards for this program.

References

[1] Smith, M., Craig, D., Herrmann, N., Mahoney, E., Krezel, J., McIntyre, N., and Goodliff, K., "The Artemis Program: An Overview of NASA's Activities to Return Humans to the Moon," *2020 IEEE Aerospace Conference*, IEEE, 2020. https://doi.org/10.1109/AERO47225.2020.9172323.

[2] Orr, J. S., Wall, J. H., VanZwieten, T. S., and Hall, C. E., "Space Launch System Ascent Flight Control Design," *2014 American Astronautical Society (AAS) Guidance, Navigation, and Control Conference*, 2014.

[3] Ahmad, N., Anzalone, E. J., Craig, A. S., and Dukeman, G. A., "Evolution and Impact of Saturn V on Space Launch System from a Guidance, Navigation, and Mission Analysis Perspective," *International Astronautical Congress (IAC)*, 2019.

[4] Hawkins, M., and Ahmad, N., "Guidance Modifications and Enhancements for Space Launch System Block-1 in Support of Artemis I and Beyond," *2020 AAS/AIAA Astrodynamics Specialist Conference*, 2020.

[5] Neal, R. M., "Probabilistic Inference using Markov Chain Monte Carlo Methods," Department of Computer Science, University of Toronto Toronto, ON, Canada, 1993.

[6] Brooks, S., "Markov Chain Monte Carlo Method and its Application," *Journal of the Royal Statistical Society: Series D*, Vol. 47, No. 1, 1998. https://doi.org/10.1111/1467-9884.00117.

[7] Godsill, S. J., "On the Relationship between Markov Chain Monte Carlo Methods for Model Uncertainty," *Journal of Computational and Graphical Statistics*, Vol. 10, No. 2, 2001.

[8] Blevins, J. A., Campbell, J. R., Bennett, D. W., Rausch, R., Gomez, R. J., and Kiris, C. C., "An Overview of the

Characterization of the Space Launch System Aerodynamic Environments," *52nd Aerospace Sciences Meeting*, 2014. https://doi.org/10.2514/6.2014-1253.

[9] Favaregh, A. L., Houlden, H. P., and Pinier, J. T., "Quantification of the Uncertainties for the Space Launch System Liftoff/Transition and Ascent Databases," *AIAA SciTech Forum 2016*, 2016. https://doi.org/10.2514/6.2016-0795.

[10] Team, S. A. T., "SLSP Vehicle Aerodynamic Data Book, Volume 1: SLS1000X," National Aeronautics and Space Administration, 2021.

[11] Houlden, H., Favaregh, A., and Hemsch, M., "Quantification of the Uncertainties for the Ares I A106 Ascent Aerodynamic Database," *27th AIAA Aerodynamic Measurement Technology and Ground Testing Conference*, 2010. https://doi.org/10.2514/6.2010-4926.

[12] Houlden, H., Favaregh, A., and Hemsch, M., "Uncertainty Quantification and Modeling for Ares I A106 Ascent Aerodynamics Database," NASA/TM-2013-218045, 2013.

[13] Kammeyer, M., "Wind Tunnel Facility Calibrations and Experimental Uncertainty," *20th AIAA Advanced Measurement and Ground Testing Technology Conference*, 1998. https://doi.org/10.2514/6.1998-2715.

[14] Belter, D., "Comparison of Wind-Tunnel Data Repeatability with Uncertainty Analysis Estimates," *20th AIAA Advanced Measurement and Ground Testing Technology Conference*, 1998. https://doi.org/10.2514/6.1998-2714.

[15] Montgomery, D. C., *Introduction to Statistical Quality Control*, 3rd ed., John Wiley & Sons, 1996.

[16] Aftosmis, M., Nemec, M., Berger, M., Chiew, J., Rodriguez, D., and Spurlock, W., *Cart3D Documentation*, 2022. URL https://www.nas.nasa.gov/publications/software/docs/cart3d/.

[17] Anderson, W. K., Biedron, R. T., Carlson, J.-R., Derlaga, J. M., Druyor Jr., C. T., Gnoffo, P. A., Hammond, D. P., Jacobson, K. E., Jones, W. T., Kleb, B., Lee-Rausch, E. M., Nastac, G. C., Nielsen, E. J., Park, M. A., Rumsey, C. L., Thomas, J. L., Thompson, K. B., Walden, A. C., Wang, L., Wood, S. L., Wood, W. A., Diskin, B., Liu, Y., and Zhang, X., *FUN3D Manual 14.0.1*, 2023. URL https://fun3d.larc.nasa.gov/.

[18] Chan, W., Gomez, R., Rogers, S., and Buning, P., "Best Practices in Overset Grid Generation," *32nd AIAA Fluid Dynamics Conference and Exhibit*, 2002. https://doi.org/10.2514/6.2002-3191.

[19] Luke, E., Tong, X., Wu, J., Tang, L., and Cinnella, P., "CHEM: A Chemically Reacting Flow Solver for Generalized Grids," *Tetra Research*, 2003.

[20] West, J., Westra, D., Lin, J., and Tucker, K., "Accuracy Quantification of the Loci-CHEM Code for Chamber Wall Heat Fluxes in a G02/GH2 Single Element Injector Model Problem," *3rd International Workshop on Rocket Combustion Modeling*, 2006.

[21] Mathelin, L., Hussaini, M. Y., and Zang, T. A., "Stochastic Approaches to Uncertainty Quantification in CFD Simulations," *Numerical Algorithms*, Vol. 38, 2005. https://doi.org/10.1007/BF02810624.

[22] Montomoli, F., Carnevale, M., D'Ammaro, A., Massini, M., and Salvadori, S., *Uncertainty Quantification in Computational Fluid Dynamics and Aircraft Engines*, Springer, 2015. https://doi.org/10.1007/978-3-319-92943-9.

[23] Salehi, S., Raisee, M., Cervantes, M. J., and Nourbakhsh, A., "Efficient Uncertainty Quantification of Stochastic CFD Problems using Sparse Polynomial Chaos and Compressed Sensing," *Computers & Fluids*, Vol. 154, 2017. https://doi.org/10.1016/j.compfluid.2017.06.016.

[24] White, L., West, T. K., Rhode, M. N., Rieken, E., Erb, A. J., Lampenfield, J., and Rodriguez, D., "CFD Validation Study of a Hypersonic Cone-Slice-Flap Configuration," *AIAA Scitech 2021 Forum*, 2021, p. 1074. https://doi.org/10.2514/6.2021-1074.

[25] Khuri, A. I., and Mukhopadhyay, S., "Response Surface Methodology," *Wiley Interdisciplinary Reviews: Computational Statistics*, Vol. 2, No. 2, 2010. https://doi.org/10.1002/wics.73.

[26] Rhode, M., Chan, D., Niskey, C., and Wilson, T., "Aerodynamic Testing of the Orion Launch Abort Tower Separation with Jettison Motor Jet Interactions," *29th AIAA Applied Aerodynamics Conference*, 2011. https://doi.org/10.2514/6.2011-3342.

[27] Chan, D. T., Paulson, J. W., Shea, P., Toro, K., Parker, P. A., and Commo, S. A., "Aerodynamic Characterization and Improved Testing Methods for the Space Launch System Liftoff and Transition Environment," *AIAA Aviation 2019 Forum*, 2019. https://doi.org/10.2514/6.2019-3398.

[28] Shea, P. R., Pinier, J. T., Houlden, H., Favaregh, A., Hemsch, M. J., Dalle, D. J., Rogers, S. E., Meeroff, J., and Lee, H. C., "Ascent Aerodynamic Force and Moment Database Development for the Space Launch System," *AIAA Aviation 2019 Forum*, 2019. https://doi.org/10.2514/6.2019-3298.

[29] Shea, P. R., "Wind Tunnel Investigation of the Ascent Aerodynamic Characteristics for a 1.3-Percent Scale Space Launch System," NASA/TM-2020-5009603, 2021.

[30] Tomek, W. G., Pinier, J. T., Houlden, H. P., Bennett, D. W., Chan, D. T., Favaregh, N. M., and Murphy, K. J., "Test Summary for 0.008-Scale Design Analysis Cycle-2 Space Launch System Force and Moment Testing in the Boeing Polysonic Wind Tunnel," NASA/TM-2018-220100, 2018.

[31] Ulbrich, N., and Volden, T., "Development of a New Software Tool for Balance Calibration Analysis," *25th AIAA Aerodynamic Measurement Technology and Ground Testing Conference*, 2006. https://doi.org/10.2514/6.2006-3434.

[32] Ulbrich, N., and Volden, T., "Regression Model Term Selection for the Analysis of Strain-gage Balance Calibration Data," *27th AIAA Aerodynamic Measurement Technology and Ground Testing Conference*, 2010. https://doi.org/10.2514/6.2010-4545.

[33] Chan, D. T., Dalle, D. J., Rogers, S. E., Pinier, J. T., Wilcox, F. J., and Gomez, R. J., "Space Launch System Booster Separation Aerodynamic Database Development and Uncertainty Quantification," *54th AIAA Aerospace Sciences Meeting*, 2016. https://doi.org/10.2514/6.2016-0798.

[34] Wilcox, F., Pinier, J. T., Chan, D. T., and Crosby, W. A., "Space Launch System Booster Separation Aerodynamic Testing at the NASA Langley Unitary Plan Wind Tunnel," *54th AIAA Aerospace Sciences Meeting*, 2016. https://doi.org/10.2514/6.2016-0796.